AIAA JOURNAL
Vol. 32, No. 11, November 1994

Finite Element for Composite Plate Bending Based on Efficient Higher Order Theory

Maenghyo Cho* and Reid Parmerter†
University of Washington, Seattle, Washington 98195

A triangular bending element based on an efficient higher order plate theory is developed for symmetric laminated composites. This nonconforming element has five degrees of freedom in each node. It passes proper bending and shear patch tests in arbitrary meshes in isotropic materials. Thus it converges to the exact solution. To demonstrate the element and compare with other theories, finite element solutions are obtained for a static bending problem under sinusoidal loading. The present finite element results give deflections and stresses that are in good agreement with three-dimensional elasticity solutions. Thus this element provides an efficient and accurate tool for the analysis of symmetric multilayered composite plates.

Introduction

RECENT research has often focused on methods of modeling multilayered composite structures and their numerical implementations (finite element). Among the possible approaches, three-dimensional and quasi-three-dimensional models are not computationally tractable. Thus researchers are pursuing more efficient methods to accurately analyze multilayered composite structures. Two-dimensional plate and shell modeling has been commonly used for its efficiency. However, in this case, it is well recognized that the transverse shear deformation effect is significant because of shear flexibility in fiber reinforced laminated composites. Therefore a Mindlin-type finite element is a popular bending element to use in analyzing composite plates. But to predict global and through-the-thickness deformation and stress distributions more accurately, a refined plate model needs to be developed. This has been the subject of a great deal of research in the past 10 years.

Phan and Reddy,[1] Putcha and Reddy,[2] Reddy and Khdeir,[3] and Kant and Pandya[4] worked to implement Reddy's simplified plate theory[5] in a finite element. Ren and Hinton[6] developed a rectangular bending element based on the modified version of the simplified plate theory.[5] Several finite element method (FEM) numerical investigations[7,8] can be found for Lo et al.[9] (LCW). The LCW cubic order theory can be implemented conveniently in the frame work of isoparametric elements. Di Sciuva[10] developed a plate bending element based on his simplified discretized plate model.[11,12] Rao and Meyer-Piening[13] developed a mixed bending element based on Toledano and Murakami's model.[14] Reddy et al.[15] developed a discretized plate bending element based on Reddy's[16] model. On the other hand, Noor and Burton[17] proposed the predictor-corrector approach, which can predict through-the-thickness stress distribution very accurately by obtaining accurate shear correction factors in a Mindlin plate model.

Simplified higher order theory and discretized theory require C^1 continuity. To satisfy the C^1 continuity condition (slope continuity), cubic Hermite functions have been introduced to ensure slope continuity as in the Kirchhoff classical plate bending element.[1,3,6,10] To circumvent the requirement of C^1 continuity, an isoparametric C^0 mixed element has been developed by introducing additional variables.[2] Kant and Pandya[4] applied transverse shear free conditions at the top and bottom surface at the finite element node level to get a C^0 element.

Recently Cho and Parmerter developed an efficient higher order plate model[18,19] that can provide accurate stress distributions. Our experience indicates this efficient higher order plate theory (EHOPT)[18,19] is a very promising method in its efficiency and accuracy. This paper addresses the question of implementing this theory in a finite element, so that plate bending problems with various loadings and boundary conditions can be analyzed.

This paper outlines the development of a triangular plate bending element. Static bending stress analyses are performed and compared with available results for other published models to assess the accuracy of the element.

Review of the Efficient Higher Order Plate Theory

The plate is composed of perfectly bounded layers with the principal material axes of each layer oriented arbitrarily with respect to the plate axes. Following the developments presented by Cho and Parmerter,[18,19] the displacements for the present theory can be written as follows for the symmetric lamination case.

Superimposing a linear zig-zag displacement field, with a different slope in each layer, on an overall cubic varying field,

$$u_\alpha = \psi_\alpha z - \frac{4}{3h^2}\left[w_{,\alpha} + \psi_\alpha + \sum_{k=1}^{N/2-1} \underline{a^k_{\alpha\gamma}(\psi_\gamma + w_{,\gamma})}\right] z^3 + \sum_{k=1}^{N/2-1} \underline{a^k_{\alpha\gamma}(\psi_\gamma + w_{,\gamma})\,[(z-z_k)H(z-z_k) - (-z-z_k)H(-z-z_k)]} \tag{1}$$

where $a^k_{\alpha\gamma}$ is a function of material properties and lamination thickness and $H(z-z_k)$ the Heaviside unit step function.

The parameters $a^k_{\alpha\gamma}$ are determined by the requirements that the transverse shear stresses vanish on the upper and lower surfaces of the plate and be continuous through the thickness of the plate, including the interface between lamina. The details of the calculation are described in Ref. 18.

Neglecting transverse normal strains, out-of-plane displacement is only a function of the in-plane coordinates.

$$u_3 = w(x_1, x_2) \tag{2}$$

If we neglect the underlined part of Eq. (1), this displacement field is the same as the one used by Levinson[20] and Reddy.[5] In fact, the displacements of the present theory are identical to Levinson's and Reddy's in the case of single-layer problems.

Presented as Paper 92-2355 at the AIAA/ASME/ASCE/AHS/ASC 33rd Structures, Structural Dynamics, and Materials Conference, Dallas, TX, April 13–15, 1992; received June 30, 1993; revision received Nov. 8, 1993; accepted for publication Nov. 20, 1993.

*Research Assistant, Department of Aeronautics and Astronautics; currently Full-Time Instructor, Department of Aerospace Engineering, Inha University, Inchon, Republic of Korea. Student Member AIAA.

†Professor, Department of Aeronautics and Astronautics, FS-10.

The constitutive equations for an orthotropic layer, in the principal axes system of the material, are

$$\begin{Bmatrix}\sigma_{11}\\ \sigma_{22}\\ \sigma_{12}\end{Bmatrix} = \begin{bmatrix}\bar{Q}_{11} & \bar{Q}_{12} & 0\\ \bar{Q}_{12} & \bar{Q}_{22} & 0\\ 0 & 0 & \bar{Q}_{66}\end{bmatrix}\begin{Bmatrix}\varepsilon_{11}\\ \varepsilon_{22}\\ \gamma_{12}\end{Bmatrix} \tag{3}$$

$$\begin{Bmatrix}\sigma_{32}\\ \sigma_{31}\end{Bmatrix} = \begin{bmatrix}\bar{Q}_{44} & 0\\ 0 & \bar{Q}_{55}\end{bmatrix}\begin{Bmatrix}\gamma_{32}\\ \gamma_{31}\end{Bmatrix} \tag{4}$$

where $\bar{Q}_{ij}$ are the plane stress reduced elastic moduli in the material axes of the layer. Since the x, y coordinate system will not, in general, be aligned with the material axes of each layer, these constitutive equations must be transformed to the x, y system in each lamina. Thus, in each lamina, the constitutive equations become

$$\begin{Bmatrix}\sigma_{11}^{(k)}\\ \sigma_{22}^{(k)}\\ \sigma_{12}^{(k)}\end{Bmatrix} = \begin{bmatrix}Q_{11} & Q_{12} & Q_{16}\\ Q_{12} & Q_{22} & Q_{26}\\ Q_{16} & Q_{26} & Q_{66}\end{bmatrix}^{(k)}\begin{Bmatrix}\varepsilon_{11}^{(k)}\\ \varepsilon_{22}^{(k)}\\ \gamma_{12}^{(k)}\end{Bmatrix} \tag{5}$$

$$\begin{Bmatrix}\sigma_{32}^{(k)}\\ \sigma_{31}^{(k)}\end{Bmatrix} = \begin{bmatrix}Q_{44} & Q_{45}\\ Q_{45} & Q_{55}\end{bmatrix}^{(k)}\begin{Bmatrix}\gamma_{32}^{(k)}\\ \gamma_{31}^{(k)}\end{Bmatrix} \tag{6}$$

where Q_{ij} are the transformed material moduli for each lamina.

By applying the virtual work principle, variational consistent equilibrium equations and boundary conditions are obtained (see Ref. 18).

Finite Element Formulation

The laminated plate theory which we have developed has second derivatives of w (transverse deflection) in the strain energy. Thus C^1 functions should be used. This condition can be conveniently implemented in rectangular elements, but difficulties arise for general quadrilaterals or triangular elements. A useful plate element should be capable of accurately modeling arbitrary boundary shapes, which rules out rectangular elements. The triangular element is the simplest that can faithfully follow curved boundaries.

However, strict enforcement of the C^1 condition introduces considerable complexity into arbitrarily oriented triangular elements. To keep the element as simple as possible a triangular nonconforming element based on the element developed by Specht[21] was adopted. This element satisfies C^1 conditions at the nodes. Along the element interface between nodes C^1 continuity is satisfied in an average rather than a pointwise sense.

The potential energy can be divided into bending and shear parts. The bending energy Π_b is expressed as

$$\Pi_b^k = \int_{z_{k-1}}^{z_k}\begin{Bmatrix}\varepsilon_1\\ \varepsilon_2\\ \gamma_{12}\end{Bmatrix}^T\begin{bmatrix}Q_{11} & Q_{12} & Q_{16}\\ Q_{12} & Q_{22} & Q_{26}\\ Q_{16} & Q_{26} & Q_{66}\end{bmatrix}^{(k)}\begin{Bmatrix}\varepsilon_1\\ \varepsilon_2\\ \gamma_{12}\end{Bmatrix} dz \tag{7}$$

$$\Pi_b = \frac{1}{2}\int_A \sum_{k=1}^{N/2} 2\Pi_b^k \, dA \tag{8}$$

The transverse shear energy Π_s is expressed as

$$\Pi_s^k = \int_{z_{k-1}}^{z_k}\begin{Bmatrix}\gamma_{23}\\ \gamma_{13}\end{Bmatrix}^T\begin{bmatrix}Q_{44} & Q_{45}\\ Q_{45} & Q_{55}\end{bmatrix}^{(k)}\begin{Bmatrix}\gamma_{23}\\ \gamma_{13}\end{Bmatrix} dz \tag{9}$$

$$\Pi_s = \frac{1}{2}\int_A \sum_{k=1}^{N/2} 2\Pi_s^k \, dA \tag{10}$$

For our three-noded triangular element, the nodal displacement vector $\{a\}^e$ is $\{w, \theta_x, \theta_y, \psi_x, \psi_y\}$ where $\theta_x = w_{,y}$ and $\theta_y = -w_{,x}$. Area coordinates L_1, L_2, and L_3 are used in the shape functions and coordinate transformation functions. Figure 1 shows geometry and coordinates of the element.

The primary displacement unknowns are expressed in terms of nodal variables and shape functions as

$$w = \sum_{i=1}^{3}\{w_i N_i + \theta_{xi} N_{xi} + \theta_{yi} N_{yi}\} \tag{11}$$

$$\psi_x = \sum_{i=1}^{3} L_i \psi_{xi}, \qquad \psi_y = \sum_{i=1}^{3} L_i \psi_{yi} \tag{12}$$

where the detailed expressions for N_i, N_{xi}, and N_{yi} are taken from Specht.[21] The terms of the basis shape functions in the area coordinate system are reproduced here, with corrections of errors made in Specht[21]

$$N_i = n_{3i-2}, \qquad N_{xi} = n_{3i-1}, \qquad N_{yi} = n_{3i} \tag{13}$$

where $i = 1$, 2, and 3.

The shape functions can be written in the form

$$n_k = \sum_{r=1}^{9} Z_{kr}^{-1} z_r \tag{14}$$

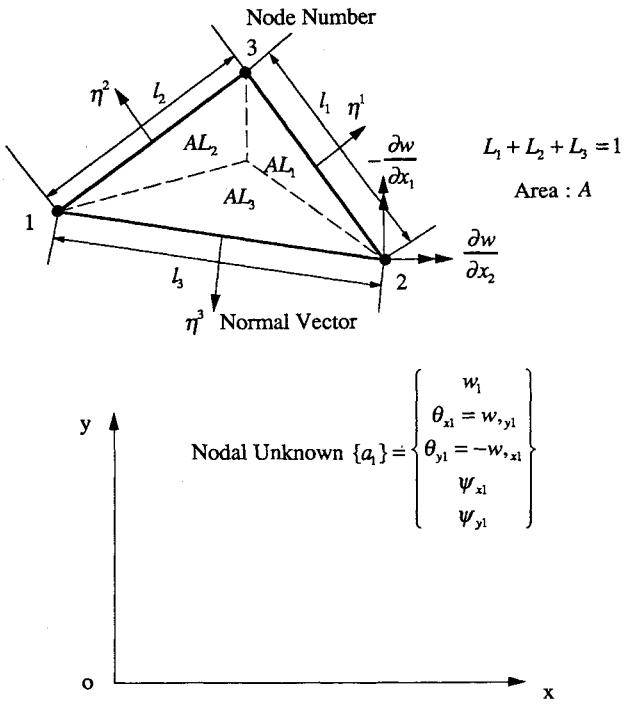

Fig. 1 Geometry and coordinates for the triangular element.

where $k = 1, \ldots, 9$ and

$$[z_r] = [L_1, L_2, L_3, L_1L_2, L_2L_3, L_3L_1,$$

$$L_1^2L_2 + (1/2)L_1L_2L_3\{3(1-\mu_3)L_1 - (1+3\mu_3)L_2 + (1+3\mu_3)L_3\},$$

$$L_2^2L_3 + (1/2)L_1L_2L_3\{3(1-\mu_1)L_2 - (1+3\mu_1)L_3(1+3\mu_1)L_1\},$$

$$L_3^2L_1 + (1/2)L_1L_2L_3\{3(1-\mu_2)L_3 - (1+3\mu_2)L_1(1+3\mu_2)L_2\}] \quad (15)$$

The constants are

$$\mu_1 = \frac{l_3^2 - l_2^2}{l_1^2} \qquad \mu_2 = \frac{l_1^2 - l_3^2}{l_2^2} \qquad \mu_3 = \frac{l_2^2 - l_1^2}{l_3^2} \quad (16)$$

where l_1, l_2, and l_3 are the lengths of the side of the triangle.

The transformation matrix Z_{kr} is regular for an arbitrary geometry of the triangle. The shape function n_k can now be set up by Eq. (14) using the inverse transformation matrix.

$$Z_{kr}^{-1} = \begin{bmatrix} 1 & 0 & 0 & -1 & 0 & 1 & 2 & 0 & -2 \\ 0 & 0 & 0 & 0 & 0 & a_{12} & -a_{13} & 0 & -a_{12} \\ 0 & 0 & 0 & 0 & 0 & a_{22} & -a_{23} & 0 & -a_{22} \\ 0 & 1 & 0 & 1 & -1 & 0 & -2 & 2 & 0 \\ 0 & 0 & 0 & a_{13} & 0 & 0 & -a_{13} & -a_{11} & 0 \\ 0 & 0 & 0 & a_{23} & 0 & 0 & -a_{23} & -a_{21} & 0 \\ 0 & 0 & 1 & 0 & 1 & -1 & 0 & -2 & 2 \\ 0 & 0 & 0 & 0 & a_{11} & 0 & 0 & -a_{11} & -a_{12} \\ 0 & 0 & 0 & 0 & a_{21} & 0 & 0 & -a_{21} & -a_{22} \end{bmatrix} \tilde{}\mu \quad (17)$$

where

$$[a_{ij}] = \left[2A\frac{\partial L_j}{\partial x_i}\right] = \begin{bmatrix} y_2 - y_3 & y_3 - y_1 & y_1 - y_2 \\ x_3 - x_2 & x_1 - x_3 & x_2 - x_1 \end{bmatrix} \quad (18)$$

which is expressed in terms of the coordinates (x_i, y_i) of the corner nodes.

In the calculation of the normal derivatives,

$$\frac{\partial}{\partial \eta^1} = \frac{l_1}{4A}\left\{\frac{\partial}{\partial L_2} + \frac{\partial}{\partial L_3} - 2\frac{\partial}{\partial L_1} + \mu_1\left(\frac{\partial}{\partial L_3} - \frac{\partial}{\partial L_2}\right)\right\} \quad (19)$$

$$\frac{\partial}{\partial \eta^2} = \frac{l_2}{4A}\left\{\frac{\partial}{\partial L_3} + \frac{\partial}{\partial L_1} - 2\frac{\partial}{\partial L_2} + \mu_2\left(\frac{\partial}{\partial L_1} - \frac{\partial}{\partial L_3}\right)\right\} \quad (20)$$

$$\frac{\partial}{\partial \eta^3} = \frac{l_3}{4A}\left\{\frac{\partial}{\partial L_1} + \frac{\partial}{\partial L_2} - 2\frac{\partial}{\partial L_3} + \mu_3\left(\frac{\partial}{\partial L_2} - \frac{\partial}{\partial L_1}\right)\right\} \quad (21)$$

where η^1, η^2, and η^3 are the normal directions to the sides of the triangle.

The global coordinates are expressed as follows:

$$x = \sum_{i=1}^{3} x_i L_i, \qquad y = \sum_{i=1}^{3} y_i L_i \quad (22)$$

Strains are expressed in terms of nodal displacements

$$\{\varepsilon_b\} = [B_b]\{a\} \quad (23)$$

where $\{\varepsilon_b\}$ is the in-plane strain which appears on the right-hand side of Eq. (6). The $\{\varepsilon_b\}$ is a 3×1 vector, $[B_b]$ is 3×15, and $\{a\}$ is 15×1.

$$\{\varepsilon_s\} = [B_s]\{a\} \quad (24)$$

where $\{\varepsilon_s\}$ is the transverse shear strain which appears on the right-hand side of Eq. (7). The $\{\varepsilon_s\}$ is a 2×1 vector and $[B_s]$ is 2×15. The potential energy can be rewritten in the compact form,

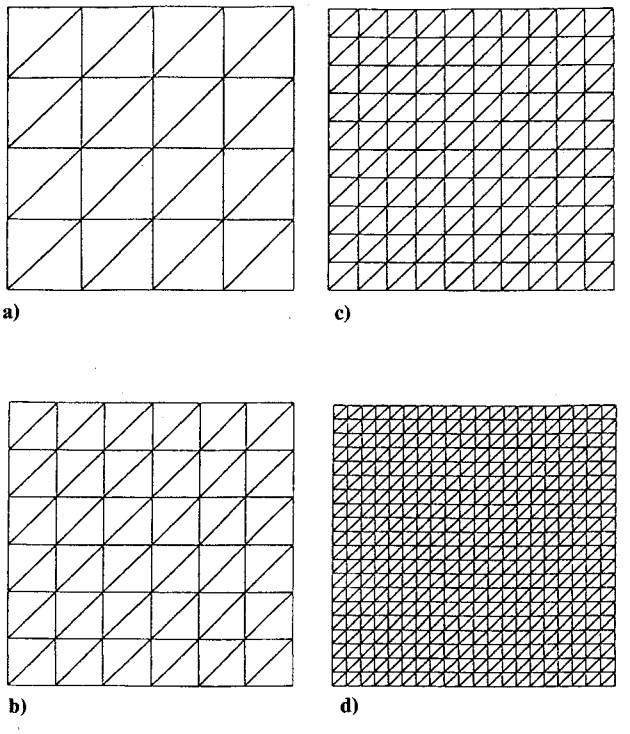

Fig. 2 Meshes used in the analysis: mesh densities a) 4×4, b) 6×6, c) 10×10, and d) 20×20.

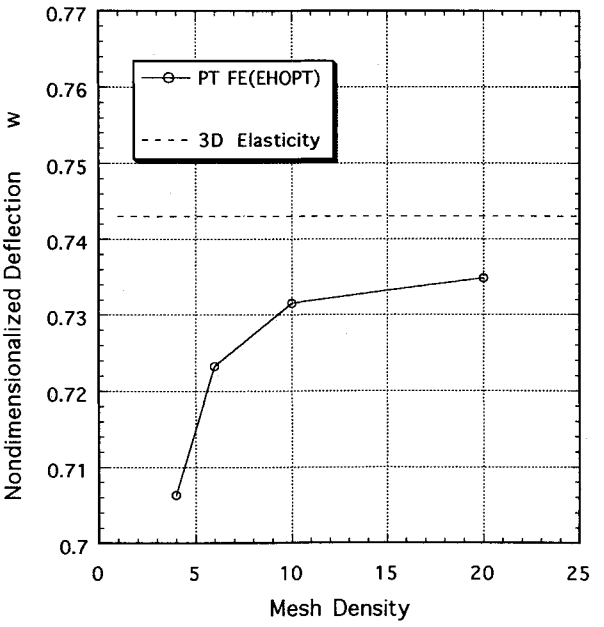

Fig. 3 Convergence rate of deflection for (0/90/90/0) cross-ply square laminates with simply supported boundary conditions under sinusoidal loading ($a/h = 10$).

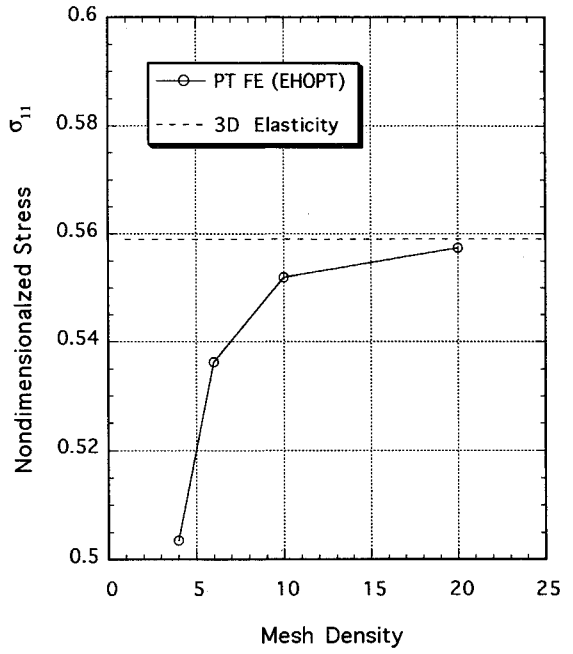

Fig. 4 Convergence rate of in-plane bending stress for (0/90/90/0) cross-ply square laminates with simply supported boundary conditions under sinusoidal loading ($a/h = 10$).

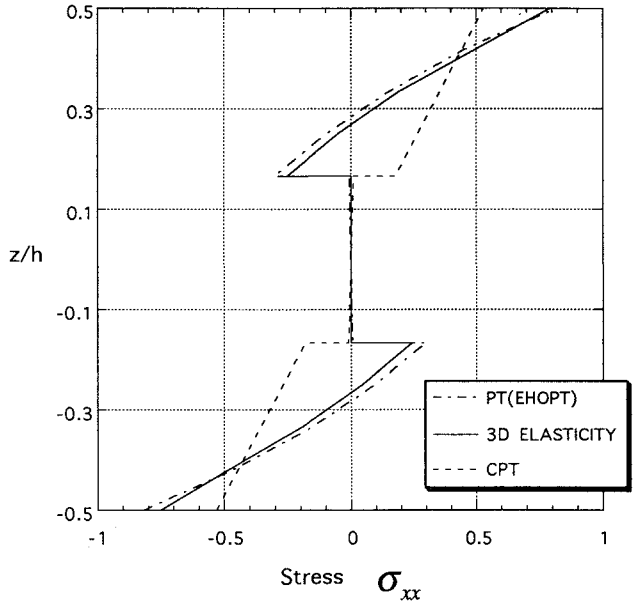

Fig. 5 Variation of the in-plane stress σ_{xx} through the thickness of three-layer cross-ply (0/90/0) laminates under sinusoidal loading ($a/h = 4$).

$$\Pi = \Pi_b + \Pi_s$$

$$= \frac{1}{2}\int_A \{a\}^T \left(\int_{-h/2}^{h/2} [B_b]^T [C_b]^k [B_b]\, dz\right) \{a\}\, dA$$

$$+ \frac{1}{2}\int_A \{a\}^T \left(\int_{-h/2}^{h/2} [B_s]^T [C_s]^k [B_s]\, dz\right) \{a\}\, dA \qquad (25)$$

where $\{a\}$ are nodal displacement vectors and $[C_b]^k$ and $[C_s]^k$ are the elastic moduli used in Eqs. (6) and (7). The element stiffness matrices are obtained by performing explicit integrations through the thickness. The lengthy and tedious expressions for $\int_{-h/2}^{h/2} [B_b]^T [C_b]^k [B_b]\, dz$ and $\int_{-h/2}^{h/2} [B_s]^T [C_s]^k [B_s]\, dz$ are omitted here. They can be found in Ref. 22.

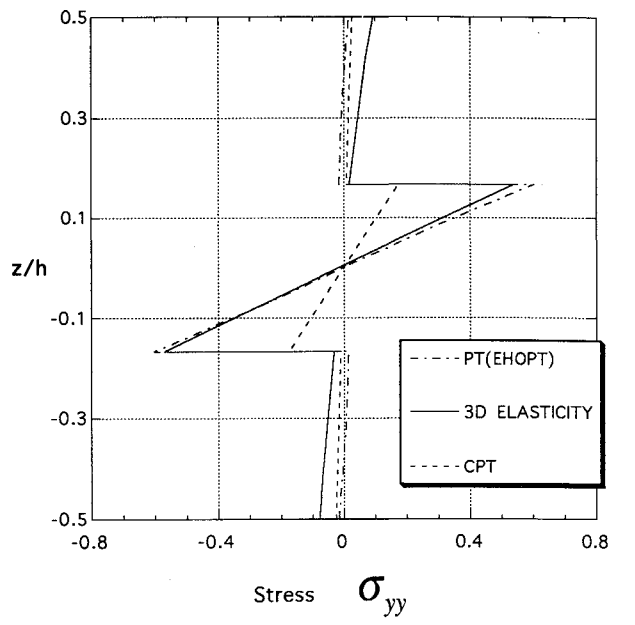

Fig. 6 Variation of the in-plane stress σ_{yy} through the thickness of three-layer cross-ply (0/90/0) laminates under sinusoidal loading ($a/h = 4$).

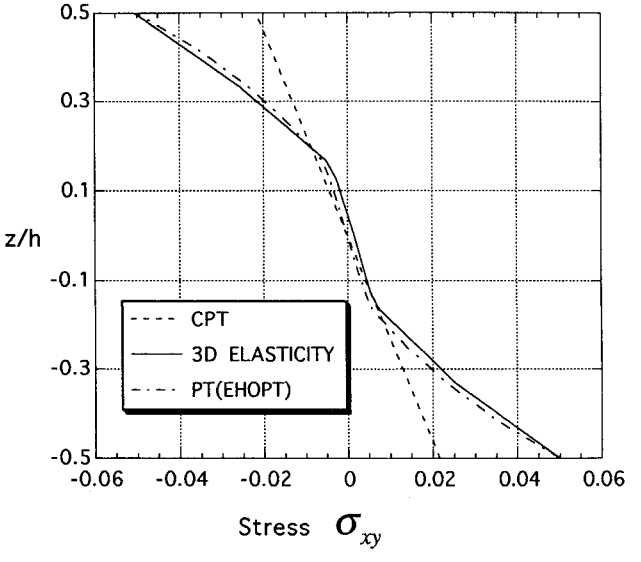

Fig. 7 Variation of the in-plane stress σ_{xy} through the thickness of three-layer cross-ply (0/90/0) laminates under sinusoidal loading ($a/h = 4$).

Patch Tests and Convergence Rates

When nonconforming elements are used, it is necessary to show that they produce solutions that converge to the true solution as the size of the elements tends to zero. Sufficient conditions for convergence are established by the proper "patch test."

Pure bending and pure shear patch tests have been performed in arbitrary meshes of an isotropic plate.[22] Full Gauss integration requires 6 points for bending and 12 for shear. However, elements with three point integration in bending and six in shear still pass the bending and shear patch tests. Therefore, these reduced integrations are used throughout the analysis for computational efficiency.

We demonstrate the rate of convergence by examining transverse deflections and axial stresses. The cross-ply (0/90/90/0) four-layer problem of the third example in the next section is considered.

Stresses are calculated at the centroid of the element and not averaged to the nodal values. Four different quadrant meshes given in Fig. 2 are used to examine the rate of convergence. As shown in

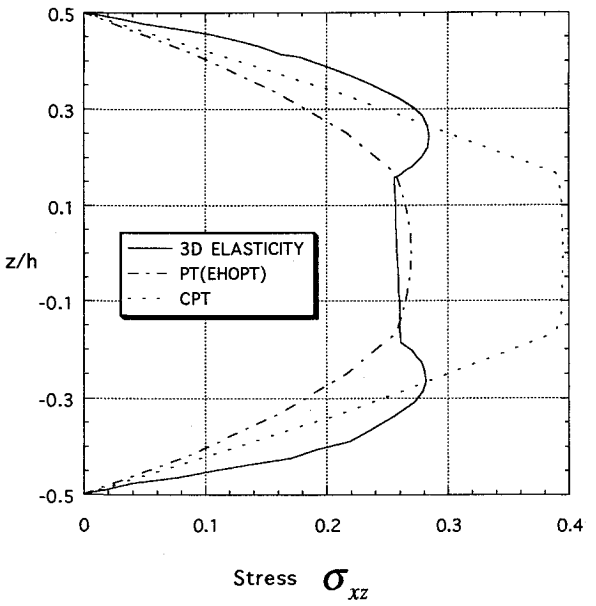

Fig. 8 Variation of the transverse shear σ_{xz} stress through the thickness of three-layer cross-ply (0/90/0) laminates under sinusoidal loading ($a/h = 4$).

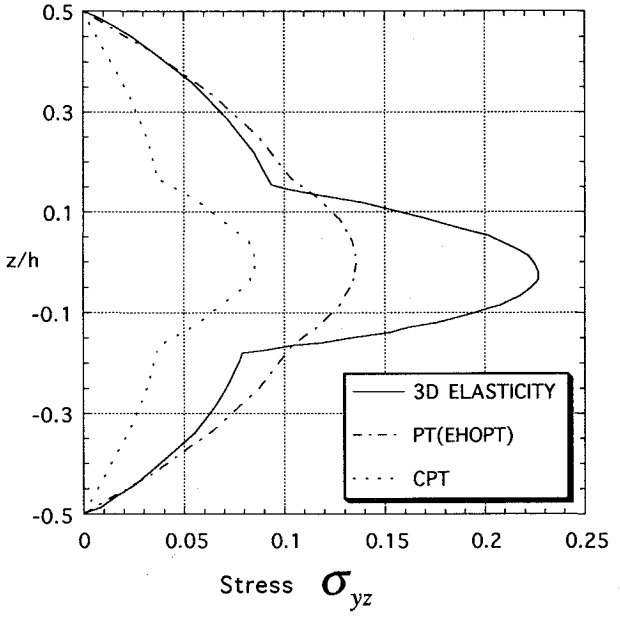

Fig. 9 Variation of the transverse shear σ_{yz} stress through the thickness of three-layer cross-ply (0/90/0) laminates under sinusoidal loading ($a/h = 4$).

Figs. 3 and 4, it is observed that the calculated deflection and stress converge monotonically to the exact solutions from the stiff side as the mesh is refined.

Numerical Results and Discussions

Numerical results for symmetric cross-ply plate problems are evaluated to assess the accuracy of the theory and the finite element described in this paper. The three-dimensional elasticity solutions of Pagano[23] and Pagano and Hatfield[24] for simply supported rectangular plates under sinusoidal loading are used for comparisons. Three examples are considered: 1) a three-layer square laminate (0/90/0) with equal ply thicknesses under a sinusoidal loading distribution, 2) a three-layer rectangular laminate (0/90/0) with aspect ratio of $b/a = 3$ under a sinusoidal loading distribution, and 3) a four-layer square laminate (0/90/90/0) with equal ply thickness under a sinusoidal loading distribution.

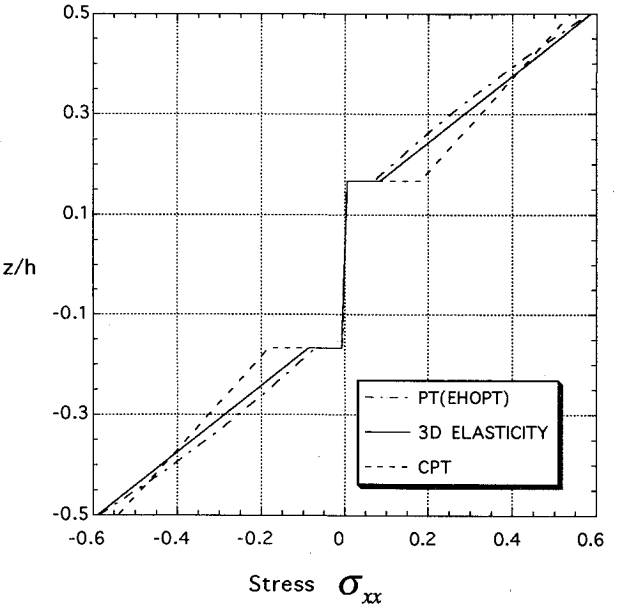

Fig. 10 Variation of the in-plane stress σ_{xx} through the thickness of three-layer cross-ply (0/90/0) laminates under sinusoidal loading ($a/h = 10$).

The material properties for the 0-deg layers are

$$E_1 = 25 \times 10^6 \text{ psi (172 GPa)}, \qquad E_2 = 1 \times 10^6 \text{ psi (6.9 GPa)}$$

$$G_{12} = G_{13} = 0.5 \times 10^6 \text{ psi (3.4 GPa)}$$

$$G_{23} = 0.2 \times 10^6 \text{ psi (1.4 GPa)}$$

$$\nu_{12} = \nu_{13} = \nu_{23} = 0.25$$

To facilitate the comparison with other theories, the following nondimensional parameters are defined for Figs. 5–14.

$$\sigma_{xx} = \frac{\sigma_{11}(a/2, b/2, h/2)}{p_0 (a/h)^2}$$

$$\sigma_{yy} = \frac{\sigma_{22}(a/2, b/2, h/2)}{p_0 (a/h)^2}$$

$$\sigma_{yz} = \frac{\sigma_{23}(a/2, 0, 0)}{p_0 (a/h)}, \qquad \sigma_{xz} = \frac{\sigma_{13}(0, b/2, 0)}{p_0 (a/h)}$$

$$\sigma_{xy} = \frac{\sigma_{12}(0, 0, h/2)}{p_0 (a/h)^2}$$

Figures 5–9 show variations of normal in-plane stresses and transverse shear stresses through the thickness under sinusoidal loading for a thickness ratio of $a/h = 4$. Figures 10–14 show the same variations for a thickness ratio of $a/h = 10$. PT(EHOPT) indicates the finite element results of the present theory (efficient higher order plate theory). For all of the examples a 10×10 mesh density is used. Three-dimensional elasticity solutions are obtained from Pagano.[23] CPT indicates classical plate theory. Stresses are calculated at the centroid of each element. Figures 5 and 10 show the comparisons of σ_{xx}. The results of the present finite element method show excellent agreement with the three-dimensional elasticity solutions. Figures 6 and 11 show σ_{yy} distributions. Although the stresses in the outer layers are not predicted as accurately as those of the inner core, the deviation from the exact elasticity solution is not significantly large.

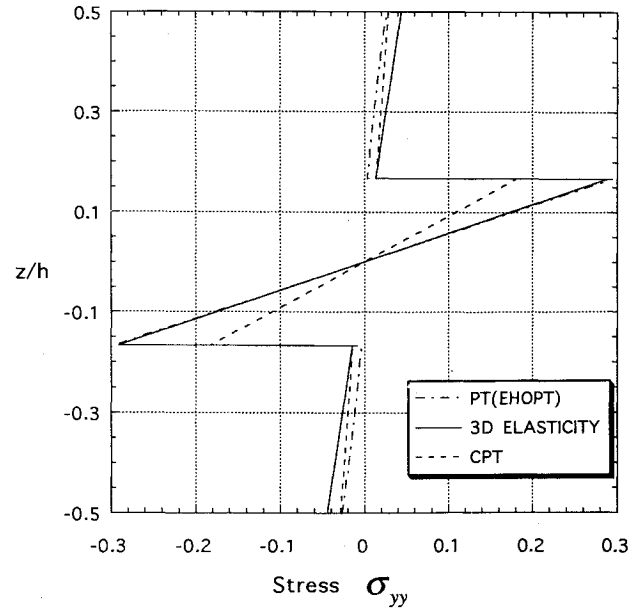

Fig. 11 Variation of the in-plane stress σ_{yy} through the thickness of three-layer cross-ply (0/90/0) laminates under sinusoidal loading ($a/h = 10$).

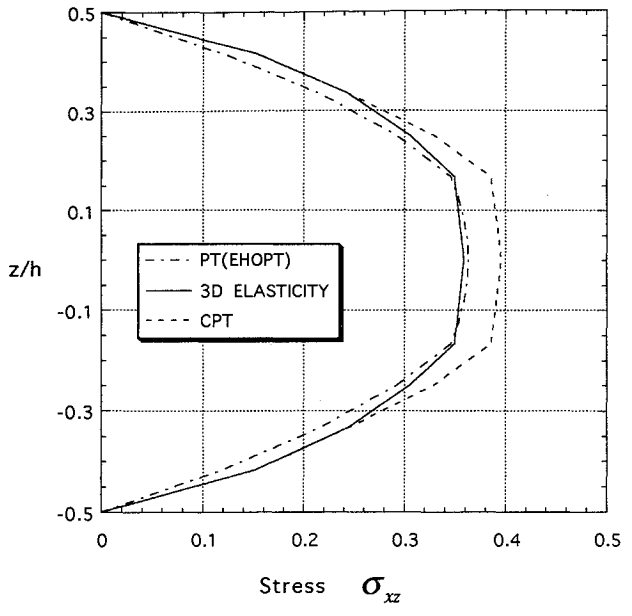

Fig. 13 Variation of the transverse shear σ_{xz} stress through the thickness of three-layer cross-ply (0/90/0) laminates under sinusoidal loading ($a/h = 10$).

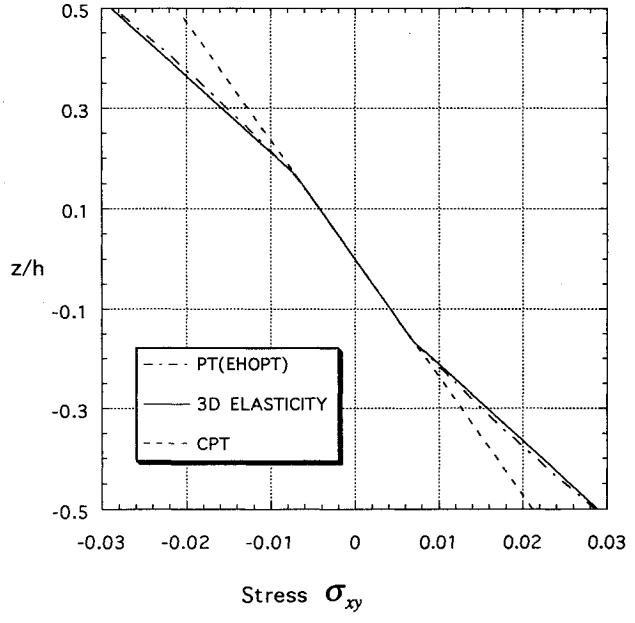

Fig. 12 Variation of the in-plane stress σ_{xy} through the thickness of three-layer cross-ply (0/90/0) laminates under sinusoidal loading ($a/h = 10$).

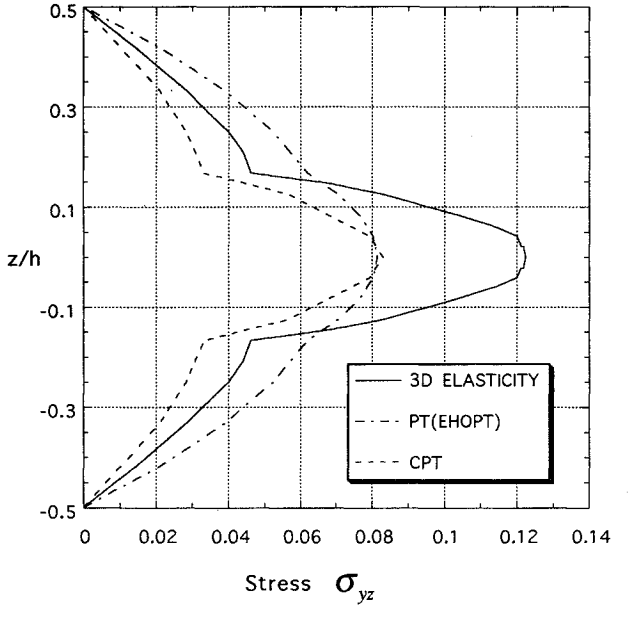

Fig. 14 Variation of the transverse shear stress σ_{yz} through the thickness of three-layer cross-ply (0/90/0) laminates under sinusoidal loading ($a/h = 10$).

Figures 7 and 12 depict the in-plane shear stress distributions through the thickness. For σ_{xx} and σ_{yy}, the stresses are discontinuous at the interfaces due to different in-plane material properties. However, in this example the in-plane shear stresses vary continuously through the thickness due to the equal in-plane shear modulus of each (0/90/0) cross-ply layer. The present in-plane shear results are in excellent accordance with those of three-dimensional elasticity.

It is well known that there are two ways of obtaining transverse shear stresses, the direct constitutive equation approach and the equilibrium equation approach. The former is convenient but usually lacks accuracy compared to the latter. The equilibrium equation approach involves higher order derivatives with respect to x and y. Thus, if higher order elements (higher than or equal to six nodes in case of triangular elements and eight nodes in quadrilateral elements) are introduced in the finite element formulation, then higher order derivatives can be calculated within each element. Since the present finite element formulation has only three nodes in each element, we face a problem in calculating higher order derivatives. This can be circumvented by a postprocess routine which calculates the higher order derivatives using least square fitting of the global nodal displacements data. These calculations were not done.

Figures 8 and 13 show transverse shear stress distribution σ_{xz}. In the very thick plate case ($a/h = 4$), the solution we obtain from constitutive equations does not follow the exact elasticity behavior point by point. But the global behavior is reasonably accurate. In the moderately thick plate case ($a/h = 10$), the result calculated by constitutive relations is fairly accurate. CPT values were obtained by the equilibrium approach. In both cases, the present constitutive approach shows better performance than the CPT results obtained by the more accurate equilibrium equation methods. With the addi-

Table 1 Center deflection $\bar{w}$ and stresses of three-layer cross-ply laminates (0/90/0) rectangular plate ($b/a = 3$) under sinusoidal loading[a]

a/h		$\bar{w}$	$\bar{\sigma}_1$	$\bar{\sigma}_2$	$\bar{\sigma}_4$	$\bar{\sigma}_5$	$\bar{\sigma}_6$
4	3-D elasticity[b]	2.82	1.10	0.119	0.0334	0.387	0.0281
	PT FE(EHOPT)[c]	2.750	1.2126	0.11205	0.025583	0.37203	0.02738
	SHOT analytic[d]	2.6411	1.0356	0.1028	0.0348	0.2724	0.0263
	First shear[e]	2.3626	0.6130	0.0934	0.0308	0.1879	0.0205
	Hybrid FE[f]	2.752	0.990	0.109	0.0380	0.387	0.0276
10	3-D elasticity	0.919	0.725	0.0435	0.0152	0.420	0.0123
	PT FE(EHOPT)	0.9178	0.7349	0.04450	0.01761	0.4340	0.01177
	SHOT analytic	0.8622	0.6924	0.0398	0.0170	0.2859	0.0115
	First shear	0.803	0.6214	0.0375	0.0159	0.1894	0.0105
	Hybrid FE	0.916	0.711	0.0366	0.0205	0.454	0.0124
100	3-D elasticity	0.508	0.624	0.0253	0.0108	0.439	0.0083
	PT FE(EHOPT)	0.5031	0.62395	0.02619	0.009361	0.5376	0.00821
	SHOT analytic	0.507	0.624	0.0253	0.0129	0.2886	0.0083
	First shear	0.5063	0.6233	0.0253	0.0127	0.1897	0.0083
	Hybrid FE	0.506	0.623	0.0229	0.0120	0.496	0.00801
	CPT	0.503	0.623	0.0252	–	–	0.0083

[a]Nondimensionalized deflections and stresses defined as
$\bar{\sigma}_1 = \sigma_{11}(a/2, b/2, h/2)/[p_0(a/h)^2]$, $\bar{\sigma}_2 = \sigma_{22}(a/2, b/2, h/2)/[p_0(a/h)^2]$
$\bar{\sigma}_4 = \sigma_{23}(a/2, 0, 0)/[p_0(a/h)]$, $\bar{\sigma}_5 = \sigma_{13}(0, b/2, 0)/[p_0(a/h)]$
$\bar{\sigma}_6 = \sigma_{12}(0, 0, h/2)/[p_0(a/h)^2]$, $\bar{w} = 100E_2h^3w(a/2, b/2, 0)/(p_0L^4)$.
[b]3-D elasticity: exact three-dimensional elasticity solution.[23]
[c]PT FE(EHOPT): present theory finite element where 10×10 mesh is used.
[d]SHOT analytic: analytical solution of simple higher order theory.[5]
[e]First shear: first-order shear deformation theory results.[5]
[f]Hybrid FE: hybrid stress finite element results.[25]

Table 2 Center deflection and stresses of four-layer square plate under sinusoidal loading[a]

a/h		$\bar{w}$	$\bar{\sigma}_1$	$\bar{\sigma}_2$	$\bar{\sigma}_4$	$\bar{\sigma}_5$	$\bar{\sigma}_6$
4	3-D elasticity	1.954	0.720	0.663	0.292	0.291	0.0467
	PT FE(EHOPT)	1.8953	0.7411	0.6974	0.2198	0.2257	0.04316
	SHOT exact	1.8937	0.6651	0.6322	0.2389	0.2064	0.0440
	First shear	1.7100	0.4059	0.5765	0.1963	0.1397	0.0308
10	3-D elasticity	0.743	0.559	0.401	0.196	0.301	0.0275
	PT FE(EHOPT)	0.7315	0.56804	0.4082	0.1462	0.3089	0.02717
	SHOT exact	0.7147	0.5456	0.3888	0.1531	0.2640	0.0268
	First shear	0.6628	0.4989	0.3615	0.1292	0.1667	0.0221
100	3-D elasticity	0.4385	0.539	0.276	0.141	0.337	0.0216
	PT FE(EHOPT)	0.4305	0.53938	0.26976	0.086141	0.2567	0.0211
	SHOT exact	0.4343	0.5387	0.2708	0.1117	0.2897	0.0213
	First shear	0.4337	0.5382	0.2705	0.1009	0.1780	0.0213

[a]Same nondimensionalization as used in Table 1, except $\bar{\sigma}_2 = \sigma_{22}(a/2, a/2, h/4)/[p_0(a/h)^2]$.

tion of postprocessing to obtain higher order derivatives, we would expect significant improvement in the transverse shear stresses calculated from our element by the equilibrium approach.

In Figures 9 and 14, transverse shear stresses σ_{yz} are presented. As shown in the figures, the present constitutive approach does not agree satisfactorily with the elasticity solutions, nevertheless, it is better than CPT using the equilibrium approach.

Tables 1 and 2 show cases 2 and 3, respectively. Stresses are calculated at the centroids of each element and smoothed to the nodal values. The present finite element method is superior in performance to both first-order shear and simple cubic shear theory.[5] It also has the same order of accuracy as the complicated layer-dependent hybrid finite element.[24]

Conclusion

A nonconforming triangular finite element for symmetric composite lamination configurations based on an efficient higher order plate theory (EHOPT) has been developed. This element passes the proper bending and shear patch tests in isotropic plates in arbitrary meshes. Some numerical examples are compared to the available exact elasticity solutions and other plate theories to demonstrate accuracy.

In the present finite element, the nodal degrees of freedom do not depend on the number of layers. For a symmetric lamination layup, only 5 degrees of freedom are needed for each node and a total of only 15 degrees of freedom for each element. Therefore, it is very efficient and accurate.

The triangular element developed here is much more suitable than existing rectangular higher order elements with C^1 continuity for solving problems involving curved boundaries such as plate bending with holes.

References

[1]Phan, N. D., and Reddy, J. N., "Analysis of Laminated Composites Using a Higher-Order Shear Deformation Theory," *International Journal for Numerical Methods in Engineering*, Vol. 21, No. 12, 1985, pp. 2201–2219.

[2]Putcha, N. S., and Reddy, J. N., "A Refined Mixed Shear Flexible Finite Element for the Nonlinear Analysis of Laminated Plates," *Computers and Structures*, Vol. 22, No. 2, 1986, pp. 529–538.

[3]Reddy, J. N., and Khdeir, A. A., "Buckling and Vibration of Laminated Composite Plates Using Various Plate Theories," *AIAA Journal*, Vol. 27, No. 12, 1989, pp. 1808–1817.

[4]Kant, T., and Pandya, B. N., "A Simple Finite Element Formulation of a Higher-Order Theory for Unsymmetrically Laminated Composite Plates," *Composite Structures*, Vol. 9, No. 3, 1988, pp. 215–246.

[5]Reddy, J. N., "A Simple Higher-Order Theory for Laminated Composite Plates," *Journal of Applied Mechanics*, Vol. 51, Dec. 1984, pp. 745–752.

[6]Ren, J. G., and Hinton, E., "The Finite Element Analysis of Homogeneous and Laminated Composite Plates Using a Simple Higher Order Theory," *Communications in Applied Numerical Methods*, Vol. 2, No. 21986, pp. 217–228.

[7]Pandya, B. N., and Kant, T., "Finite Element Analysis of Laminated Composite Plates Using a Higher-Order Displacement Model," *Composite Science and Technology*, Vol. 32, No. 2, 1988, pp. 137–155.

[8]Kant, T., Ravichandran, R. V., Pandya, B. N., and Mallikarjuna, "Finite Element Transient Dynamic Analysis of Isotropic and Fiber Reinforced Composite Plates Using a Higher-Order Theory," *Composite Structure*, Vol. 9, No. 4, 1988, pp. 319–342.

[9]Lo, K. H., Christensen, R. M., and Wu, E. M., "A Higher-Order Theory of Plate Deformation, Part 2: Laminated Plates," *Journal of Applied Mechanics*, Vol. 44, Dec. 1977, pp. 669–676.

[10]Di Sciuva, M., "Evaluation of Some Multilayered, Shear-Deformable Plate Elements," *Computers and Structures*, Vol. 24, No. 6, 1986, pp. 845–854.

[11]Di Sciuva, M., "Bending, Vibration and Buckling of Simply Supported Thick Multilayered Orhtotropic Plates: An Evaluation of a New Displacement Model," *Journal of Sound and Vibration*, Vol. 105, No. 3, 1986, pp. 425–442.

[12]Di Sciuva, M., "An Improved Shear Deformation Theory for Moderately Thick Multilayered Anisotropic Shells and Plates," *Journal of Applied Mechanics*, Vol. 54, Sept. 1987, pp. 589–596.

[13]Rao, K. M., and Meyer-Piening, H.-R., "Analysis of Thick Laminated Anisotropic Composite Plates by the Finite Element Method," *Composite Structures*, Vol. 15, No. 3, 1990, pp. 185–213.

[14]Toledano, A., and Murakami, H., "A High Order Laminated Plate Theory with Improved In-Plane Responses," *International Journal of Solids and Structures*, Vol. 23, No. 1, 1987, pp. 111–131.

[15]Reddy, J. N., Barbero, E. J., and Teply, J. L., "A Plate Bending Element Based on a Generalized Laminated Plate Theory," *International Journal for Numerical Methods in Engineering*, Vol. 28, No. 10, 1989, pp. 2275–2292.

[16]Reddy, J. N., "A Generalization of Two-Dimensional Theories of Laminated Plates," *Communications in Applied Numerical Methods*, Vol. 3, No. 3, 1987, pp. 173–180.

[17]Noor, A. K., and Burton, W. S., "Stress and Free Vibration Analyses of Multilayered Composite Plates," *Composite Structures*, Vol. 14, No. 3, 1990, pp. 233–265.

[18]Cho, M., and Parmerter, R. R., "An Efficient Higher Order Plate Theory for Laminated Composites," *Composite Structures*, Vol. 20, No. 2, 1992, pp. 113–123.

[19]Cho, M., and Parmerter, R.R., "An Efficient Higher Order Composite Plate Theory for General Lamination Configuration," *AIAA Journal*, Vol. 31, 1993, pp. 1299–1306.

[20]Levinson, M., "An Accurate Simple Theory of the Statics and Dynamics of Elastic Plates," *Mechanics Research Communications*, Vol. 7, No. 6, 1980, pp. 343–350.

[21]Specht, B., "Modified Shape Functions for the Three-Node Plate Bending Element Passing the Patch Test," *International Journal for Numerical Methods in Engineering*, Vol. 26, No. 3, 1988, pp. 705–715.

[22]Cho, M., "An Efficient Higher Order Theory for Laminated Composite Plates and a Finite Element Implementation," Ph.D. Dissertation, Dept. of Aeronautics and Astronautics, Univ. of Washington, Seattle, WA, 1993.

[23]Pagano, N. J., "Exact Solutions for Rectangular Bidirectional Composites and Sandwich Plates," *Journal of Composite Materials*, Vol. 3, July, 1969, pp. 398–411.

[24]Rao, K. M., and Meyer-Piening, H.-R., "Analysis of Sandwich Plates Using a Hybrid-Stress Finite Element," *AIAA Journal*, Vol. 29, No. 9, 1991, pp. 1498–1506.